Reconfigurable Curved Beams for Selectable Swimming Gaits in an Underwater Robot

Mohammad Sharifzadeh, Yuhao Jiang, and Daniel M. Aukes

***Abstract*—Rowing is a swimming motion employed by a number of animals via tuned passive biomechanics and active gait strategies. This gait generates positive net thrust (or moment) by having a higher drag profile in the power stroke compared with the recovery stroke, which is obtained via faster actuation speed or higher effective area. In this letter, we show that using the preferential buckling of curved beams in swimming robots can, via a passive reduction of effective area in recovery stroke, be used to generate positive net thrust and moment. Additionally, these curved beams can be actively tuned to alter their behavior on demand for use in swimming applications, and can be used in an underwater robot to switch between rowing and flapping gaits. A dynamic model has been developed to model the swimming behavior of a robot using buckling joints. A design optimization has been carried out, using the Covariance Matrix Adaption Evolution Strategy (CMA-ES), to find the design and gait parameters that maximize the robot's forward swimming speed. A series of experimental gait searches have subsequently been conducted on the resulting optimal design, again using CMA-ES with the goal of finding the optimal gait pattern across a number of swimming strategies such as paddling, flapping, and undulation. By actively altering the curved beam's buckling limits, an untethered robot has been developed that maneuvers in water across each of these swimming strategies. The findings suggest that tuning the preferential buckling limits of curved beams can be an effective and potentially advantageous approach for producing directional thrust and moments.**

***Index Terms*—Compliant joints and mechanisms, soft robot materials and design, soft robot applicationsc, modeling, control, and learning for soft robots.**

I. Introduction

THIS letter explores the role curved surfaces and local buckling can play in creating rowing motions for use in underwater swimming. More specifically, we present a design concept featuring an under-actuated compliant fin system that leverages slender curved beams and their ability to buckle preferentially in one direction under symmetric motor inputs to produce net thrust and moments, as seen in Fig. 1. Furthermore, this letter aims to demonstrate the advantages of the proposed fin system in terms of its simplicity, modelability, and tuneability. This is accomplished via dynamic modeling and simulation, design and input gait optimization, as well as experimental evaluation of a swimming robot that utilizes the proposed fin design to enhance maneuverability by switching between rowing and flapping gaits across different swimming scenarios.

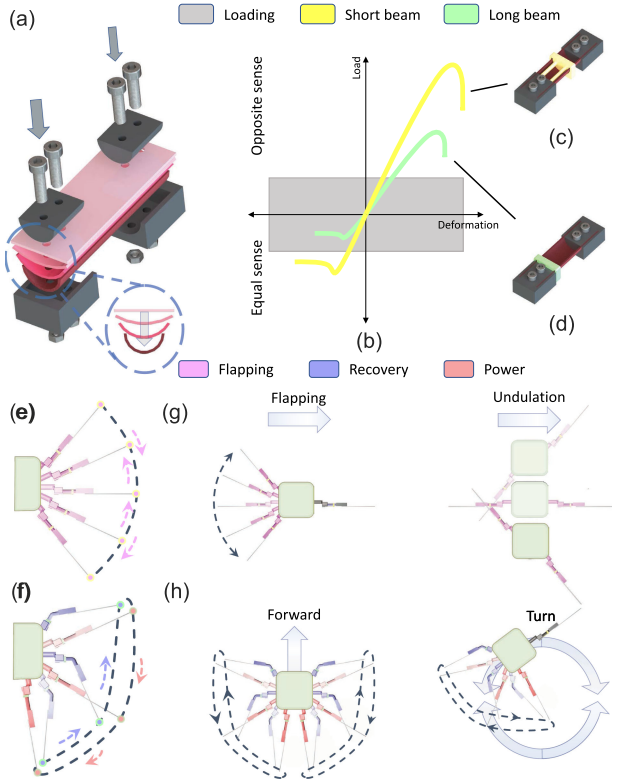

Fig. 1. Utilizing curved beams in rowing and flapping swimming strategies. (a) Curving mechanism. (b) The nonlinear behavior of curved beams. (c) short beam. (d) long beam. (e) flapping gait. (f) Rowing gait. (g) Lateral swimming using one fin flapping gait, and undulation. (h) Forward swimming and turning using rowing gait.

Underwater creatures exhibit several fascinating swimming behaviors; among them are feathering, rowing and flapping motions that occur in at least three different phyla. Rowing as a locomotion strategy is characterized by reciprocating motions directed in parallel with the direction of travel, while flapping is typified by motions exerted perpendicular to the direction of travel [1]. Feathering is an alternative to rowing that leverages pitching [2], making this motion more complex to model and

Manuscript received October 15, 2020; accepted February 6, 2021. Date of publication March 4, 2021; date of current version March 23, 2021. This letter was recommended for publication by Associate Editor G. Endo and Editor C. Gosselin upon evaluation of the reviewers' comments. This work was supported by the National Science Foundation under Grant 1935324. *(Corresponding author: Daniel Aukes.)*

Mohammad Sharifzadeh and Daniel M. Aukes are with the Polytechnic School, Fulton Schools of Engineering, Arizona State University, Mesa, AZ 85212 USA (e-mail: sharifzadeh@asu.edu; danaukes@asu.edu).

Yuhao Jiang is with the School for Engineering of Matter, Transport and Energy, Fulton Schools of Engineering, Arizona State University, Tempe, AZ 85281 USA (e-mail: yuhao92@asu.edu).

This letter has supplementary downloadable material available at https://doi.org/10.1109/LRA.2021.3063961, provided by the authors.

Digital Object Identifier 10.1109/LRA.2021.3063961

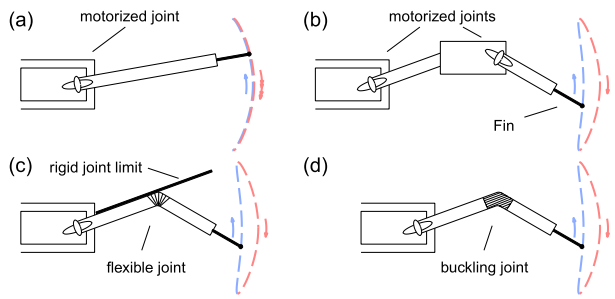

Fig. 2. Comparison between different methods to achieve net thrust in rowing. (a) Variable speed actuation (b) multiple motorized joints. (c) Passive flexible joint with a hard stop. (d) Compliant joint leveraging a curved beam.

fabricate compared with the planar motions of rowing. Among animals that use a rowing strategy, such as the beach flea [3], backswimmer [4], and copepod [5], fish have been studied more extensively [2], [6]; more robotic platforms leveraging rowing inspired by fish can be found in literature as well. Fish oscillate their paired pectoral fins to generate thrust in their "labriform" swimming mode, and number of approaches are used by roboticists to mimic this style of swimming. In some cases, a faster power stroke and slower recovery stroke produces nonzero net thrust or moment [7], [8] at the cost of potentially increased control complexity and prolonged recovery strokes (Fig. 2(a)). Another approach uses a multi-actuation system to reconfigure for recovery [9], [10] (Fig. 2(b)). This approach introduces the trajectory hysterisis needed but can suffer from higher complexity as well as a heavier and less efficient system. Soft robotic approaches have more recently been used to demonstrate the use of flexible hinges as well. For example, flexible joints or fins are used alongside rigid joint limits to produce positive net thrust and moment (Fig. 2(c)) [11]–[13]. The deformation of flexible joints during recovery repositions the fin to reduce drag, while rigid joint limits prevent bending during the power stroke, keeping the fin system better-positioned to push against the surrounding fluid. This approach, while effective at reducing control complexity, is not actively reconfigurable.

In contrast to prior solutions, passive rowing is achieved in this letter by taking advantage of the nature of flexible curved beams to preferentially buckle within a rowing cycle (Fig. 2(d)). This fin system design produces net thrust and moments through symmetric sinusoidal actuation of a single actuator, resulting in a simple and energy efficient approach. Moreover, the unique characteristics of slender curved beams provide us with the opportunity to tune the system's dynamic behavior (Fig. 1) by altering its stiffness. As demonstrated below, by changing the effective length of a curved beam, we can inhibit buckling unidirectionally or bi-directionally, enabling us to switch between a rowing gait with a net forward thrust (when actuated as a pair) and a flapping gait, generating lateral thrust. When a pair of such fins are used together, a number of other swimming modalities may be observed as well. This tunability, which is made possible through internal reconfiguration of the buckling beam, splits the use of actuators according to their purpose – power and reconfiguration, permitting us to use machine-learning approaches to find optimal gaits for different swimming modalities in a decoupled fashion, where tuning actuators are first determined, with a subsequent, independent optimization of the power actuator signal.

Buckling is a condition where small geometric perturbations lead to drastic reductions in load-carrying capacity in structural systems. Though potentially useful in mechanisms, it has not been extensively utilized for robotic locomotion. Some prior work investigates buckling and snap-through instabilities in mechanical devices. In [14], a self-deployed gliding wing is made using characteristics of a curved origami facet. These curved facets permit wings to deploy at the device's ballistic apex, resulting in an increased gliding range. Baek *et al.* extend the use of a similar self-deployed wing in a ladybird beetle-inspired jump-gliding robot [15]. In [16], an origami-inspired structure is used to produce dual-stiffness joints by pre-stretching and sandwiching a flexible material in a multi-layer structure during fabrication to induce buckling in the presence of high forces, forming a mechanical fuse.

In contrast to prior work, our work seeks to leverage the simplicity of slender curved beams as passive, nonlinear elements in the active cyclic generation of thrust and moments. In prior work [17], the authors demonstrated that with symmetric flapping actuation, buckling beams can be used to generate forward thrust, power, and work, validated through experimental data that measures the forces produced by wings flapping in air and water. Here, we extend the previous study by demonstrating how tuning the effective length of a curved beam can be used to reconfigure gaits to mimic a number of swimming motions found in biology. We also carry out an optimization of a number of design parameters as well as the actuation signal using an evolutionary approach in conjunction with a dynamic simulation; this is validated with an experimental approach to understand the change in forces generated by the system as well as the ability of a robotic system to swim freely using these different modes.

The contributions of this letter include (i) the concept of using length change to reconfigure the stiffness profile of a curved beam to preferentially buckle; (ii) the use of this mechanism to switch between rowing and flapping gaits in a mobile robot; (iii) a new dynamic model that simulates robot swimming by integrating the nonlinear stiffness of curved flexible beam joints; (iv) the use of that model, in addition to an experimental platform, in the optimization of the robot's design as well as its actuation signal by using an evolutionary approach (CMA-ES); and (v) experimental validation of the forces and trajectories estimated during optimization on a prototype of the proposed platform.

We believe this concept fits within a larger class of soft elements which we call Soft, Curved, Reconfigurable, Anisotropic Mechanisms (SCRAMs). Among prior work grouped around this concept, notable examples include a mechanism that uses pinching within tubular structures to induce highly directional changes in stiffness [18], and an underactuated limb design that incorporates hysteretic, pre-curved joints to change their response during loading and unloading [19].

The remainder of the letter is arranged in the following order: we first describe the unique characteristics of curved beams enhancing our fin design. We then discuss a dynamic model for the proposed fin design and justify its use by validating it

against experimental data. The model is subsequently used to estimate swimming distance across different designs and actuation signals with an optimization pipeline using CMA-ES. After prototyping the selected design from the prior step, we conduct an experimental search for the actuation signals across rowing, flapping, and undulatory gaits. Finally, based on the obtained results, a swimming robot is fabricated, and its swimming is studied. The letter concludes in Section VI with thoughts on impact and future work.

II. Design & Fabrication

This section details curved beams and their nature to buckle preferentially, for use in creating rowing and flapping gaits. A flat, slender, compliant beam shows little resistance towards bending; however, by inducing curvature in it (Fig. 1(a)), the resulting curved beam resists bending in the direction opposing its camber (known as opposite sense bending) more than when the beam is bent in the direction of the beam's camber (equal sense bending). The influence of curvature results in different buckling limits in equal and opposite sense bending as well. Furthermore, this phenomenon is also controllable by considering the effective length of the beam (green and yellow lines in Fig. 1(b)). When the beam's effective length is shorter, both the stiffness and buckling behavior behave more symmetrically, while at the same time, beam stiffness increases.

In this study, we use this controllable, asymmetric buckling behavior to enhance swimming in an underwater robot. We show that by careful consideration during mechanical design, the preferential buckling of curved beams can be used to passively produce a rowing gait even with simple, symmetric inputs. On the other hand, the beam can also be reconfigured to produce flapping gaits. As shown by the green plot in Fig. 1(b), in the rowing gait regime, the fluid's dynamic load on the distal end of a properly-sized beam (Fig. 1(d)) overcomes its critical buckling limit in equal sense bending, resulting in the beam undergoing a large deflection during recovery stroke (blue in Fig. 1(f)). Buckling permits the fin to travel nearly parallel with the direction of motion, rather than perpendicular to it, altering the angle of attack to reduce drag on the fin during the recovery stroke. In the power stroke, however, the fluid's dynamic load on a properly-dimensioned curved beam does not exceed the critical buckling limit in the opposite sense; the beam consequently remains perpendicular to the direction of motion, maintaining higher drag forces on the distally-mounted fin (red in Fig. 1(f)). Cycles of alternating power and recovery strokes result in a rowing gait that can be used to produce a positive net thrust in the forward direction. In the flapping regime, by shortening and stiffening the curved beam (Fig. 1(c)), the critical buckling limits of the beam – in both equal and opposite sense bending – are larger than the fluid's dynamic load (yellow plot in Fig. 1(b)), resulting in a flapping gait that primarily produces lateral thrust (Fig. 1(e)).

One of the common formulations to describe the buckling phenomenon of curved beams in literature is the behavior of folded tape-springs [20]–[24]. The behavior of a tape spring is formulated by Wuest in [23], in which moment-curvature relationships for a tape spring subject to equal and opposite end moments are obtained. Soykasap states that end moments can be obtained by integrating moments about the transverse axis for the whole cross-section of the tape spring by considering the beam as a slightly distorted axi-symmetric cylindrical shell and provides formulations to calculate the critical buckling moments in opposite and equal sense bending. In [20], Soykasap's formulation also assumes that materials are operating in their linear regime and that the loading on the distal end of curved beams is a pure moment. In our case, both material properties of the polyester beam and its loading condition caused by fluid dynamics do not satisfy the assumptions. In [17], we have previously shown that a beam's curvature influences and can be used to increase the difference between opposite and equal sense critical loads using Finite Element Analysis (FEA). We have also shown with FEA in [17] that the opposite and equal-sense critical buckling loads are much closer in value in shorter beams. This has been verified experimentally, by measuring the torque/rotation behavior and identifying the critical loads for the long and short beams corresponding to the device depicted in Fig. 1(c), (d).

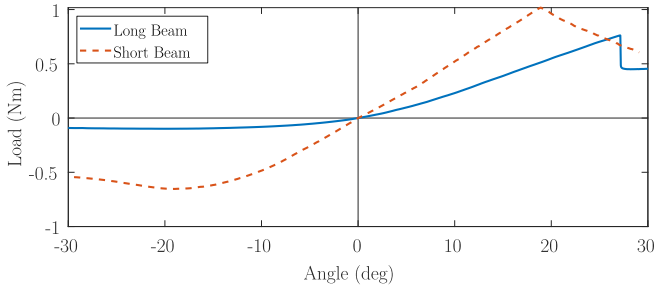

Fig. 3. Experimental data showing the changing nonlinear behavior of curved beams with a short and long effective length. The positive x-axis represents opposite-sense bending, while the negative x-axis represents equal-sense bending.

Fig. 3 shows the nonlinear behavior of two specimens with the same curvature (180°) and width (25.4 mm), and with effective lengths of 31.75 and 3.6 mm. In this test, for each specimen, the curved beam is attached at one end to a fixed plate while a known force is applied to the other end. A force sensor mounted to the output of a linear actuator pushes on the beam via a small, 3D printed contact point. The linear actuator moves back and forth through a 50 mm range in 10 μm increments while forces and torques are logged. Since the curved beams are modeled as a flexible hinge, the sampled data is displayed by their equivalent torque and defo rmation angles in Fig. 3. These profiles are used within subsequent models and prototypes in the rest of this letter. These data also show that by reducing the beam length, the critical buckling limit in equal sense bending increases from 0.1 to 0.65 Nm; the limit for opposite sense buckling, however, only increases from 0.76 to 1.02 Nm. Thus, for fluid-dynamic loads between 0.1 to 0.65 Nm, altering the effective length changes the buckling condition from unidirectional to bi-directional, resulting in the gait switching from rowing to flapping.

A slider mechanism has been implemented to alter the effective length of the beam, as illustrated in Fig. 6 b. The mechanism

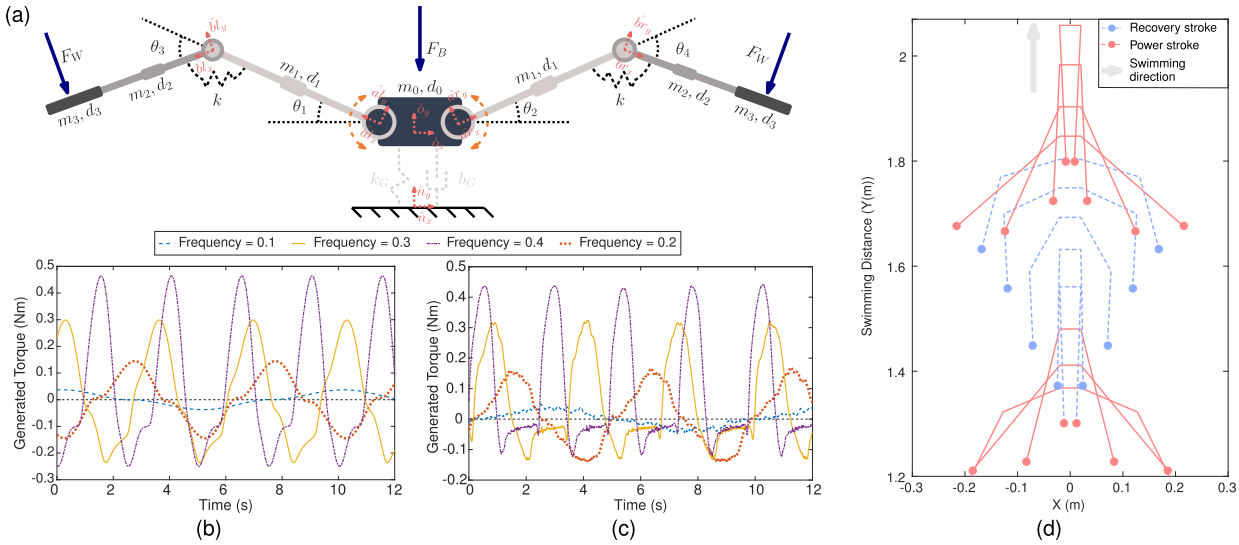

Fig. 4. Dynamic modeling of the robot swimming in water with long effective length. (a) Model for the swimming robot. Torque exerted by the wing on the frame, when the robot is fixed, from simulation (b) and experiment (c). (d) Simulation of robot swimming freely without any constraints.

consists of a rigid slider with a curved slot; when pulled, it prevents deflection by maintaining the beam's curvature, decreasing the length of the portion of the beam available to buckle. The slider's neutral configuration is set by a compression spring as the beam's natural length, which permits one-sided buckling – and thus rowing – at lower forces. To activate flapping, a single actuator pulls both fins' sliders forward via a tendon and pulley system, preventing buckling when the beams are loaded. The curved beam's stiffness in this configuration is both higher and more symmetric (in the equal and opposite sense), as seen in the red dashed line in Fig. 3.

III. Dynamic Modeling

In order to optimize the design of the device for rowing, we next describe the dynamics of the system by considering the contribution of the wing's drag, the curved beam's stiffness (in the long configuration), and the inertial effects of each body. The proposed robot uses two fins attached to the main robot's body at a distance of d_0 (shown in Fig. 4(a)). Each fin is represented by two rigid links (d_1, m_1 and d_2, m_2) with point masses located at their centers of mass, connected by a pin joint and torsional spring, with stiffness coefficient of K, connected in parallel. The nonlinear stiffness of the spring is represented by three linear regimes; the slopes of each of these regimes have been adjusted to best fit experimental data collected from our specimen in its long effective length configuration (blue in Fig. 3). Using the flat plate model, the forces on a fin due to a fluid are estimated by using equations derived from [25]:

$$F_w = \rho u^2 A \sin\alpha, \tag{1}$$

where ρ, u, A, and α are the density of fluid, the relative velocity of the plate, the area of the plate, and the angle-of-attack of the wing, respectively. α is 0 when parallel to the flow and 90° when perpendicular (in 2D) [25]. This force is perpendicular to the wing and acts as the fluid's dynamic load on the distal end of curved beam.

Using (1), we can use the velocity of the plate (u) to control the amount of drag force exerted on it, which, in conjunction with the load limits determined by the mechanics of the curved buckling beam, determines whether and under what conditions buckling occurs. Though the flat plate model best describes the fluid dynamics of a system when the Reynolds number is low and the system is in the laminar regime, we previously compared the flat plate model with the results of a Computational Fluid Dynamics (CFD) analysis on the system wing in [17], and showed that, in the worst case, the maximum error between flat plate model and CFD results is less than 15%. Due to the simplicity of the flat plate model, we use it in our simulation to reduce computation time and keep the optimization process tractable. Our simulation is performed with a Python-based dynamics package called Pynamics. This library derives the Equation of Motion (EOM) using Kane's method [26].[1] which are then integrated using the scipy.integrate.odeint() function to determine the system's state over time. The performance of the model is evaluated by comparing the moments generated by one fin against data collected experimentally. By defining two forces connecting the robot to the ground (k_G and b_G in Fig. 4(a)), the forces and moments exerted on the environment about the rotational axis when one fin is actuated may be measured in simulation.

When a sinusoidal input torque is applied to the base joint of a fin, the dynamic model demonstrates that the wing system transitions between a non-buckling flapping regime to a one-sided buckling regime when the input frequency increases. Fig. 4 b plots the torque across different input frequencies as a function of time. From these data, we can see that the wing system transitions from the non-buckling regime to one-sided buckling at around 0.3 Hz, where the maximum positive torque

[1]https://github.com/idealabasu/code_pynamics.git

TABLE I
TORQUES (IN NM) GENERATED IN SIMULATION AND EXPERIMENT

Frequency	Simulation		Experiment		Buckling
	$\tau_{\min}$	$\tau_{\max}$	$\tau_{\min}$	$\tau_{\max}$	
0.1	-0.04	0.04	-0.04	0.04	No
0.2	-0.14	0.14	-0.14	0.15	No
0.3	-0.23	0.3	-0.13	0.32	One side
0.4	-0.24	0.46	-0.12	0.44	One side

TABLE II
PARAMETER RANGE IN DESIGN AND INPUT OPTIMIZATION

Parameter	Range	Parameter	Range
d_0 (mm)	40 - 160	d_1 (mm)	30 - 160
d_2 (mm)	30 - 160	d_3 (mm)	30 - 160
α (deg)	0 - 90	β (deg)	-90 - 90
f (Hz)	0.1 - 1.2	ϕ (deg)	0 - 359

increases with frequency in the power stroke, but the maximum negative torque in the recovery section remains low. Fig. 4 c shows the moments exerted on a force sensor attached to the robot's main body when similar inputs are commanded to the robot using our experimental setup explained in (Section V). Table I(d)ata also shows an acceptable correlation between the generated torques in this experiment and the values estimated by the dynamic model. Based on this performance, we simulate the robot swimming by removing the forces holding the robot's main body ($k_G = b_G = 0$). We also consider a drag force acting on the main body for more realistic simulation. Fig. 4(d) shows a time sequence of the robot's motion when both fins are actuated with a symmetric input gait and robot swims forward; the recovery and power strokes are illustrated in blue and red, respectively.

IV. DESIGN OPTIMIZATION

Using the dynamic model introduced above, we next seek the design that maximizes forward swimming speed for symmetric rowing gaits. In our optimization, we consider the lengths of the fin's links and the distance between the robot's drive motors as design parameters (d_1, d_2, d_3 and d_0 in Fig. 4). The mass of each link is based on measurements of physical prototypes. Any optimization focusing solely on design parameters would be incomplete; actuator inputs are thus optimized simultaneously. The torques at motorized joints track desired angular trajectories ($\theta_1 \& \theta_2$ in Fig 4(a)) via k_G and b_G as mentioned previously. Input signals are supplied as a pair of sinusoidal functions,

$$\begin{aligned} \theta_1 &= \beta_1 + \alpha_1 \sin(2\pi f_1 t) \\ \theta_2 &= \beta_2 + \alpha_2 \sin(2\pi f_2 t + \phi), \end{aligned} \tag{2}$$

where θ_i is actuator i's angle, and β_i, α_i, f_i, and ϕ_i are the sinusoidal signals' angular offset, amplitude, frequency and phase shift, respectively. In order to have synchronized rowing gaits for the purposes of forward rowing, these parameters are set to $\alpha_1 = -\alpha_2$, $\beta_1 = -\beta_2$, $f_1 = f_2$, and $\phi = 0$. Based on the design and input gaits parameters introduced above, there are seven parameters affecting the robot's swimming speed. We have selected a numerical optimization approach using an evolution strategy for finding the optimal parameters; while the whole parameter space may be searched for lower-dimensional problems, we utilize CMA-ES as a way to find ideal parameters within this seven-dimensional space, as finding a globally-optimal solution would be neither be feasible nor desirable.

CMA-ES is an evolution strategy that uses stochastic methods to numerically solve nonlinear and non-convex optimization problems [27]. Using an evolution strategy like CMA-ES in practical experiments has many advantages in comparison with other meta-heuristic and search-based algorithms [28]. The main disadvantage of CMA-ES is its computational complexity, which derives from the self-adaptation and decomposition of the covariance matrix [29]. CMA-ES has been employed as an optimization tool in robotics due to its short evaluation time compared to other strategies [30], which has practical benefits including increasing the service life of motors, bearings, and gears that can become worn or damaged during training.

In our optimization process, we define the cost function as negative of the swimming range that robot achieves in 10 seconds. We also introduce the following assumptions and constraints to simplify the optimization process and obtain more realistic results:

Assumptions: (i) Water drag is applied to the main body and fins (F_B and F_W in Fig. 4), but not to the links. (ii) Drag is applied to the center of each geometry. (iii) Fins and main body have rectangular cross-sections with 80 and 50 mm widths, respectively. (iv) The robot body's mass, mostly driven by the mass of servos and electronics, is assumed to be constant.

Constraints: (i) Variables remain within the ranges defined by Table II. (ii) The total length of the robot is under 560 mm (to fit our water tank). (iii) Actuation speed and power must remain within the servo's nominal speed and power range. (iv) Loads on the curved beam must remain below opposite sense critical load throughout the trial. (v) Design and gait parameters must not collide during actuation.

We have defined a penalty function in order to exclude non-feasible solutions, in which a large positive value proportional to the number of violated constraints is returned. The penalty function gradually restricts the large search space to converge within the feasible solution space of the problem. For feasible solutions, the dynamic simulation runs and the cost function returned.

Fig. 5 a shows the cost function value as well as the evolution of the design throughout the CMA-ES optimization process for the parameter sets that exhibit a noticeable reduction in the cost value. The results converged after 25 iterations, revealing that designs with a smaller distance between the fins (d_0) as well as smaller second link length (d_2) are preferential for maximizing swimming speed. Figures 5(b,c) show cost function values for feasible parameter sets. The optimal design parameters (in mm) are $d_0 = 40\, d_1 = 112.1, d_2 = 30.2,$ and $d_3 = 114.2$.

We have designed a prototype using the above design parameters (Fig. 6(b)). The lengths of the rigid parts are calculated assuming that the curved beam bends at the midpoint. This assumption is made based on the observation of the curved beam bending underwater. Two Hitec D646WP waterproof servos

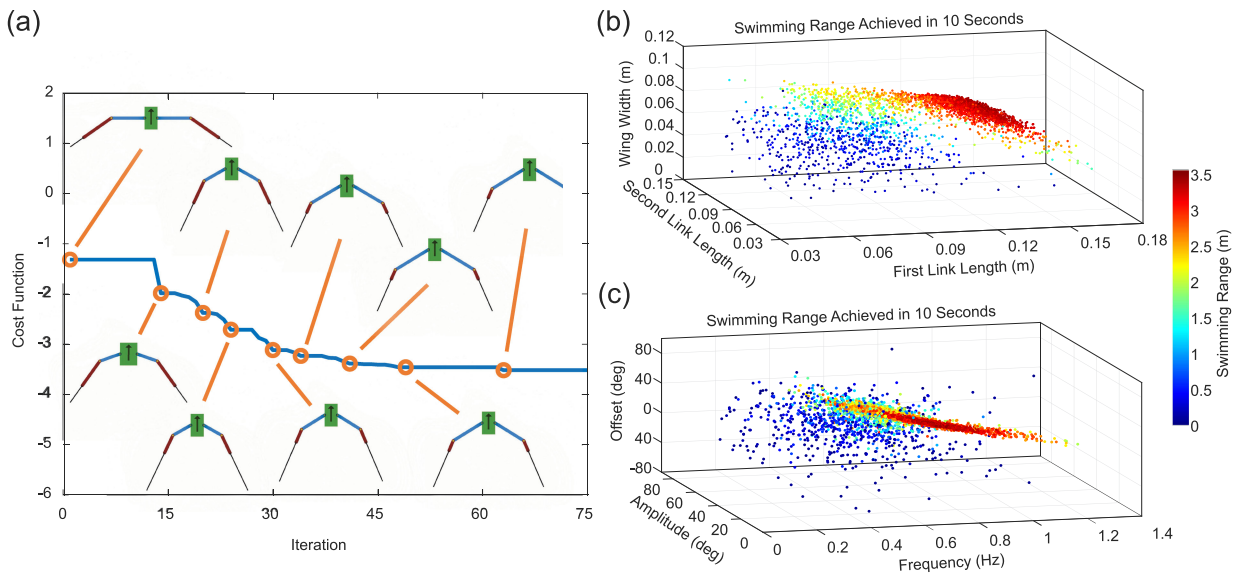

Fig. 5. Design optimization using the dynamic model. (a) The value of optimization cost function and the evolution of the robot design. Feasible parameter sets in the optimization process: (b) Fin system design parameters and (c) input gaits.

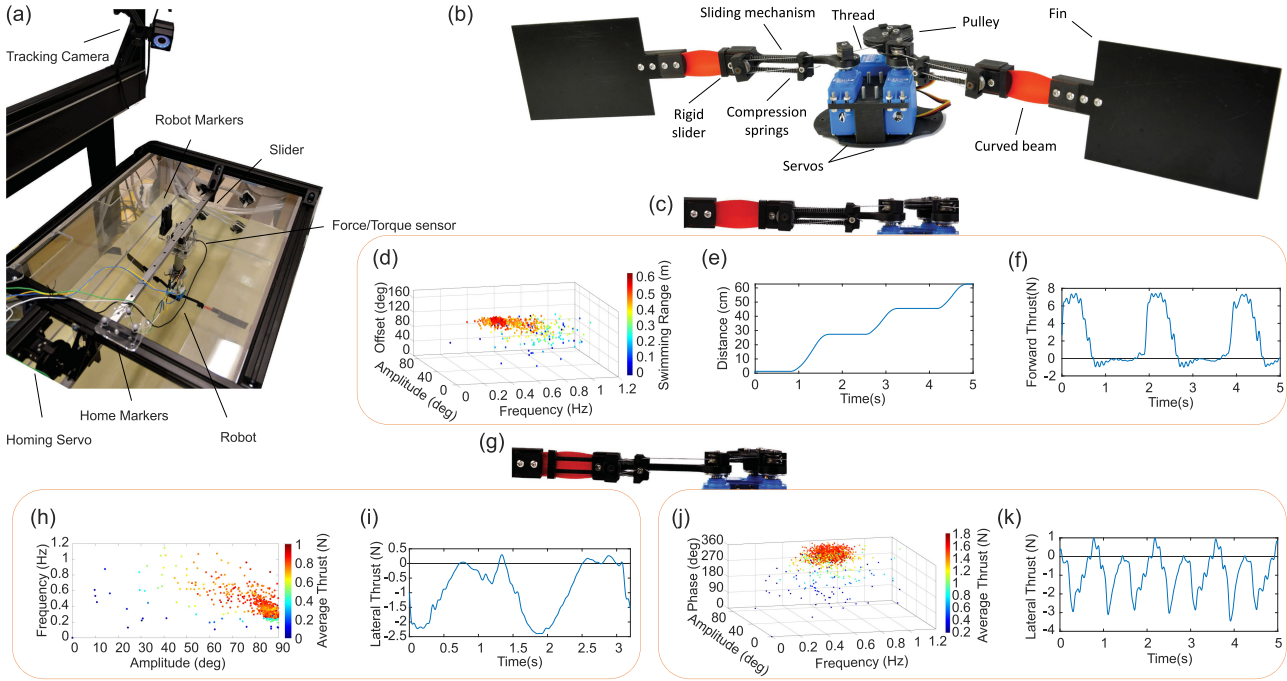

Fig. 6. Results of the experimental gait optimization for (c–f) forward swimming, (g–i) lateral swimming, and (g,j–k) undulation. (a) Experimental setup. (b) Robot's prototype. Sliding mechanism configuration for (c) Long and (g) short effective lengths. (e) Position vs. time for forward swimming. (f,i,k) Thrust forces generated by each gait.

actuate the input joints; the rigid links are 3D printed from Onyx;[2] the fin is cut from 0.76 mm fiberglass sheets.[3]

V. Experimental Gait Optimization

This section describes our approach to experimentally search for optimal gaits for various swimming maneuvers using the final prototype, which was based on the optimal results from the prior simulation. The experimental search is essential for closing the gap between simulation and real-world trials due to model estimation errors caused by the flat plate model, as well as the approach used for modeling servo control. To evaluate the performance of each gait, we have prepared an experimental setup (Fig 6(a)) capable of sampling either the thrust and moment generated by the fins, or the swimming distance and speed. A linear carriage running on a rail is installed on the top of a $4 \times 2 \times 2\,\text{ft}^3$ tank ($\text{l} \times \text{w} \times \text{h}$). The robot's position is measured using

[2]markforged.com
[3]acpcomposites.com

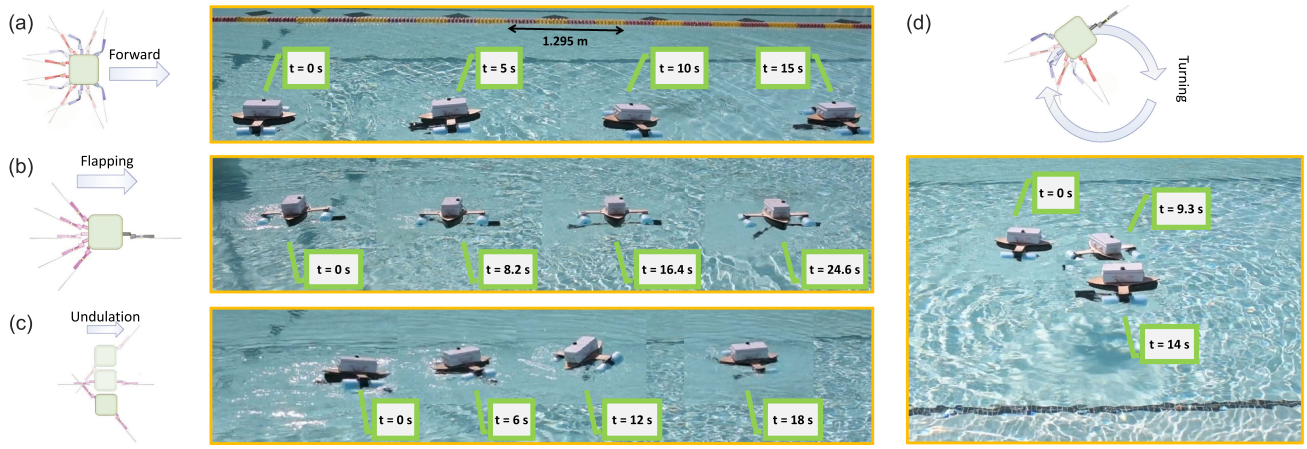

Fig. 7. Untethered robot swimming. (a) Swimming forward using rowing gaits of both fins. (b) Swimming laterally using one fin flapping actuation. (c) Swimming using undulating gait. (d) Turning by rowing gaits of one fin.

an OptiTrack motion tracking system. An ATI mini-40 force-torque sensor is attached to the carriage; its distal attachment connects to the robot via a an aluminum extension arm that holds the robot underwater. An optimization process is then performed using CMA-ES to find the optimal parameters of each desired gait by determining optimal parameters for control rule (2).

Rowing Gaits: In this optimization process, the robot swims 5 seconds with the buckling beam in its long configuration (Fig. 5(c)); the distance traveled in that time is then measured. A servo and pulley resets the carriage to its initial position at the end of each trial. In order to protect the curved beams from damage due to gaits that exceed a safe operating range, a joint limit is temporarily attached during the optimization process, and optimal gaits are then re-tested once they are determined to be safe. Fig. 6(d) shows the swimming distance for the feasible parameter sets in the optimization process. The swimming distance of the best gait is illustrated in Fig. 6(e). The data show a discontinuous pattern motion. We believe this is caused by high friction and stiction within the linear slider; the generated thrust measurements may be seen in Fig. 6(f). Nevertheless, the data also shows the efficacy of the one-sided buckling of the curved hinge when used in conjunction with optimized input gaits to generate net thrust; the forces generated during recovery stroke are limited to -1 N, while the power stroke achieves 7.5 N thrust at its peak.

Flapping Gaits: By reducing the effective length of the curved beam (Fig. 6(g)), its stiffness increases in both the opposite and equal-sense directions, changing the buckling beam's behavior, seen in Fig3, to be both stiffer and more symmetric. Using this phenomenon, lateral thrusts may be generated by flapping one limb ($\alpha_2 = \beta_2 = f_2 = 0$) with a sinusoidal input while maintaining a neutral offset in the other ($\beta_1 = 0$). A new set of optimal gait parameters was obtained by searching through the resulting two-dimensional space of gait parameters, but the lateral thrust found by this approach was unable to overcome rail stiction. We therefore adopted a thrust-based metric (rather than a distance metric) similar to [6]. Figures 6(h,i) illustrate the average thrust generated by each gait throughout the optimization as well as the thrust generated by the optimal gait, respectively. The result shows that a flapping gait with relatively large input amplitude ($\alpha = 87°$) and low frequency ($f = 0.3$ Hz) is optimal.

By commanding both limbs to perform asynchronous, symmetric flapping gaits ($\phi \neq 0°$), the robot swimming mode changes to undulation, similar to snakes, eels, and Purcell's three-link swimmer [31]–[33]. We have experimentally searched the three-dimensional space of input parameters related to undulation in order to obtain the highest lateral thrust undulating gait that exceeds the lateral single-limb maximum swimming speed found above. The resulting net thrust generated by each set of gait parameters throughout the optimization is shown in Fig. 6(j); the optimal gait generated thrust is shown in Fig. 6(k).

To address the problem of stiction which we found in the experimental setup, a free-swimming prototype has been constructed by mounting the swimming mechanism to a floating platform that ensures the fins stay underwater, while keeping power electronics above the water. Using the optimal gaits obtained from the experimental search, the untethered robot's performance has been evaluated (Fig 7).

Using the optimal rowing gait, the robot achieves a forward swimming speed of about 0.32 m/s (Fig 7(a)); the swimming distance per rowing cycle is around 0.6 m. The robot is also able to turn when only one limb is commanded by the same optimal gait. The turning speed is 25.7 deg/s (Fig 7(d)). When flapping, the untethered robot achieves a lateral swimming speed of 0.17 m/s when only one limb is actuated (Fig 7(b)). When undulating, the robot achieves a swimming speed of 0.16 m/s (Fig 7(c)). It was observed that, while the thrust data is better for an undulating strategy, the swimming speed of the untethered robot was lower than others, which we attribute to the higher drag of the floating platform when rotating. Future work will consider this additional loss of energy in modeling and optimization.

VI. Conclusions & Future Work

This letter studies how altering the stiffness and buckling limits of slender curved beams enhances swimming maneuverability by providing the opportunity to switch between different swimming gaits. By introducing a dynamic model that simulates

the swimming of a robot using this concept, we have performed a design optimization to increase swimming speed. We have also conducted an experimental search through selected gait parameters for swimming strategies that result in a robot that is capable of swimming both forward and laterally as well as turning. The unique characteristics of our fin system, obtained through the use flexible curved beams, not only simplifies the role actuation plays in locomotion, but also helps decouple the role of the actuators between the generation of work and reconfiguration. We believe our approach of tuning stiffness and buckling limits, in conjunction with simple actuation strategies, will eventually permit lower-power and more affordable robots to be tuned for specialist jobs in niche environments, while still permitting a wide range of locomotion strategies.

Future work will focus on improving models to include three-dimensional simulation for better understanding the full state of underwater robot dynamics, as well as implementing depth change. This will enable us to consider multiple swimming strategies simultaneously in optimizing the robot's body and fin morphology We also plan to continue optimizing the design of curved beam devices for more efficient locomotion by investigating variable stiffness designs as well as multi-material fabrication strategies. Future work will expand this concept further to include terrestrial locomotion and amphibious environments.

REFERENCES

[1] J. A. Walker and M. W. Westneat, "Kinematics, dynamics, and energetics of rowing and flapping propulsion in fishes," *Integrative Comp. Biol.*, vol. 42, no. 5, pp. 1032–1043, 2002.

[2] G. V. Lauder and B. C. Jayne, "Pectoral fin locomotion in fishes: Testing drag-based models using three-dimensional kinematics," *Amer. Zoologist*, vol. 36, no. 6, pp. 567–581, 1996.

[3] S. Sudo, T. Amano, A. Shirai, and T. Hayase, "On the motility and locomotive organs of beach flea," *J. Aero Aqua Bio-mechanisms*, vol. 4, no. 1, pp. 37–43, 2015.

[4] C. Essenberg, "The habits and natural history of the backswimmers notonectidae." *J. Animal Behav.*, vol. 5, no. 5, pp. 381–390, 1915.

[5] E. S. Fanta, "Anatomy of the nauplii of oithona ovalis herbst (copepoda, cyclopoida)," *Boletim de Zoologia , Univ. S. Paulo*, vol. 1, pp. 205–238, 1976.

[6] G. V. Lauder and P. G. Madden, "Fish locomotion: Kinematics and hydrodynamics of flexible foil-like fins," *Experiments Fluids*, vol. 43, no. 5, pp. 641–653, 2007.

[7] S. B. Behbahani, J. Wang, and X. Tan, "A dynamic model for robotic fish with flexible pectoral fins," in *Proc. IEEE/ASME Int. Conf. Adv. Intell. Mechatronics*., 2013, pp. 1552–1557.

[8] F. A. Naser and M. T. Rashid, "Design, modeling, and experimental validation of a concave-shape pectoral fin of labriform-mode swimming robot," *Eng. Rep.*, vol. 1, no. 5, 2019, Art no. e 12082.

[9] N. Kato, B. W. Wicaksono, and Y. Suzuki, "Development of biology-inspired autonomous underwater vehicle" bass iii" with high maneuverability," in *Proc. Int. Symp. Underwater Technol. (Cat. No 00EX418)*., 2000, pp. 84–89.

[10] P. E. Sitorus, Y. Y. Nazaruddin, E. Leksono, and A. Budiyono, "Design and implementation of paired pectoral fins locomotion of labriform fish applied to a fish robot," *J. Bionic Eng.*, vol. 6, no. 1, pp. 37–45, 2009.

[11] S. B. Behbahani and X. Tan, "Design and modeling of flexible passive rowing joint for robotic fish pectoral fins," *IEEE Trans. Robot.*, vol. 32, no. 5, pp. 1119–1132, Oct. 2016.

[12] A. Simha, R. Gkliva, Ü. Kotta, and M. Kruusmaa, "A flapped paddle-fin for improving underwater propulsive efficiency of oscillatory actuation," *IEEE Robot. Automat. Lett.*, vol. 5, no. 2, pp. 3176–3181, Apr. 2020.

[13] V. A. Pham, T. T. Nguyen, B. R. Lee, and T. Q. Vo, "Dynamic analysis of a robotic fish propelled by flexible folding pectoral fins," *Robotica*, vol. 38, no. 4, pp. 699–718, 2020.

[14] S.-M. Baek, D.-Y. Lee, and K.-J. Cho, "Curved compliant facet origami-based self-deployable gliding wing module for jump-gliding," in *Proc. ASME Int. Des. Eng. Tech. Conf. Comput. Inf. Eng. Conf. ACM*, 2016.

[15] S.-M. Baek, S. Yim, S.-H. Chae, D.-Y. Lee, and K.-J. Cho, "Ladybird beetle-inspired compliant origami," *Sci. Robot.*, vol. 5, no. 41, 2020, pp. 1–10.

[16] S. Mintchev, J. Shintake, and D. Floreano, "Bioinspired dual-stiffness origami," *Sci. Robot.*, vol. 3, no. 20, 2018, Art no. eaau0275.

[17] M. Sharifzadeh and D. M. Aukes, "Curvature-induced buckling for flapping-wing vehicles," *IEEE/ASME Trans. Mechatronics*, vol. 26, no. 1, pp. 503–514, Feb. 2021.

[18] Y. Jiang, M. Sharifzadeh, and D. M. Aukes, "Reconfigurable soft flexure hinges via pinched tubes," in *Proc. IEEE/RSJ Int. Conf. Intell. Robots Syst.*, 2020, pp. 8843–8850.

[19] M. Jiang, R. Song, and N. Gravish, "Knuckles that buckle: Compliant underactuated limbs with joint hysteresis enable minimalist terrestrial robots," in *Proc. IEEE/RSJ Int. Conf. Intell. Robots Syst.*, Las Vegas, NV, USA, 2020, pp. 3732–3738, Accepted.

[20] Ö. Soykasap, "Analysis of tape spring hinges," *Int. J. Mech. Sci.*, vol. 49, no. 7, pp. 853–860, 2007.

[21] S. J. I. Walker and G. S. Aglietti, "Experimental investigation of tape springs folded in three dimensions," *AIAA J.*, vol. 44, no. 1, pp. 151–159, 2006.

[22] S. Hoffait, O. Brüls, D. Granville, F. Cugnon, and G. Kerschen, "Dynamic analysis of the self-locking phenomenon in tape-spring hinges," *Acta Astronautica*, vol. 66, no. 7–8, pp. 1125–1132, 2010.

[23] W. Wuest, "Einige anwendungen der theorie der zylinderschale," *ZAMM-J. Appl. Math. Mechanics/Zeitschrift für Angewandte Mathematik und Mechanik*, vol. 34, no. 12, pp. 444–454, 1954.

[24] K. Seffen, "On the behavior of folded tape-springs," *J. Appl. Mechanics*, vol. 68, no. 3, pp. 369–375, 2001.

[25] J. W. Roberts, R. Cory, and R. Tedrake, "On the controllability of fixed-wing perching," in *Proc. Amer. Control Conf.*, no. 1, 2009, pp. 2018–2023. [Online]. Available: http://ieeexplore.ieee.org/document/5160526/

[26] T. R. Kane and D. A. Levinson, *Dynamics, Theory and Applications*. New York, NY, USA: McGraw Hill, 1985.

[27] N. Hansen, "The CMA evolution strategy: A comparing review," *Towards A New Evolutionary Computation*. Berlin, Germany: Springer, 2006, pp. 75–102.

[28] S. Doncieux, N. Bredeche, J.-B. Mouret, and A. E. G. Eiben, "Evolutionary robotics: What, why, and where to," *Front. Robot. AI*, vol. 2, no. 4, pp. 1–18, 2015.

[29] M. N. Omidvar and X. Li, "A comparative study of cma-es on large scale global optimisation," in *Proc. Australas. Joint Conf. Artif. Intell*. Berlin, Germany: Springer, 2010, pp. 303–312.

[30] F. Veenstra, J. Jørgensen, and S. Risi, "Evolution of fin undulation on a physical knifefish-inspired soft robot," in *Proc. Genet. Evol. Comput. Conf.*, 2018, pp. 157–164.

[31] R. L. Hatton, Y. Ding, H. Choset, and D. I. Goldman, "Geometric visualization of self-propulsion in a complex medium," *Phys. Rev. Lett.*, vol. 110, Feb. 2013, Art no. 0 78101.

[32] E. M. Purcell, "Life at low reynolds number," *Amer. J. Phys.*, vol. 45, no. 1, pp. 3–11, 1977.

[33] L. E. Becker, S. A. Koehler, and H. A. Stone, "On self-propulsion of micro-machines at low reynolds number: Purcell's three-link swimmer," *J. Fluid Mechanics*, vol. 490, pp. 15–35, 2003.